Gas kinematics of a sample of five Hickson Compact Groups. The data

Philippe Amram, Henri Plana, Claudia Mendes de Oliveira, Chantal Balkowski, J. Boulesteix

A&A 402, 865–877 (2003)
DOI: 10.1051/0004-6361:20030034

Astronomy & Astrophysics

Gas kinematics of a sample of five Hickson Compact Groups⋆,⋆⋆

The data

P. Amram[1], H. Plana[2], C. Mendes de Oliveira[3], C. Balkowski[4], and J. Boulesteix[1]

[1] Observatoire Astronomique Marseille-Provence & Laboratoire d'Astrophysique de Marseille, 2 place Le Verrier, 13248 Marseille Cedex 04, France
[2] Observatorio Nacional MCT, Rua General Jose Cristino 77, São Cristóvão, 20921-400 Rio de Janeiro, RJ, Brazil
[3] Universidade de São Paulo, Instituto de Astronomia, Geofísica e Ciências Atmosféricas, Departamento de Astronomia, Rua do Matão 1226, Cidade Universitária, 05508-900, São Paulo, SP, Brazil
[4] Observatoire de Paris, GEPI, CNRS and Université Paris 7, 5 place Jules Janssen, 92195 Meudon Cedex, France

Received 9 October 2002 / Accepted 19 December 2002

Abstract. We present Fabry Perot observations of galaxies in five Hickson Compact Groups: HCG 10, HCG 19, HCG 87, HCG 91 and HCG 96. We observed a total of 15 galaxies and we have detected ionized gas for 13 of them. We were able to derive 2D velocity, monochromatic, continuum maps and rotation curves for the 13 objects. Almost all galaxies in this study are late-type systems; only HCG 19a is an elliptical galaxy. We can see a trend of kinematic evolution within a group and among different groups – from strongly interacting systems to galaxies with no signs of interaction – HCG 10 exhibits at least one galaxy strongly disturbed; HCG 19 seems to be quite evolved; HCG 87 does not show any sign of merging but a possible gas exchange between two galaxies; HCG 91 could be accreting a new intruder; HCG 96 exhibits past and present interactions.

Key words. galaxies: kinematics and dynamics – galaxies: evolution – galaxies: interactions – galaxies: ISM – galaxies: formation – galaxies: intergalactic medium

1. Introduction

Hickson Compact Groups (hereafter collectively referred to as HCGs) are collections of three to seven galaxies inside a three-magnitude interval, where the members have a projected separation of the order of the galaxy diameters (Hickson 1992). The original photometric selection criteria found spectroscopic confirmation for 92% of the group candidates (Hickson et al. 1992). With a low velocity dispersion (~200 km s^{-1}), Hickson Compact Groups are a privileged laboratory to study different stages of interactions from violent interacting systems to systems with no apparent signs of interaction.

Galaxies in compact groups of galaxies (hereafter referred to as CGGs) are galaxies (1) which live in the most dense environments of the nearby universe (2) which experience a high rate of galaxy-galaxy interactions and (3) which are probably also progenitors of galaxies in formation (tidal dwarf galaxy candidates formed in heavily interacting systems) and in that sense, they mimic the early universe. Nevertheless, they are different from the first galaxies because they are generally large galaxies.

In 1995, we began an observation program using a Fabry-Perot instrument to obtain 2D-velocity maps of CGG with the aim of investigating the influence of the dense environments of compact groups on the kinematics and dynamics of their member galaxies. The goals of this study are: (1) to classify the groups in different evolutionary stages (merging groups, strongly interacting groups, weakly interacting groups, non-groups and single irregular galaxies); (2) to build the Tully-Fisher relation for CGGs and (3) to search for tidal dwarf galaxy candidates.

Such a study is the extension of a previous effort in the same lines, in order to determine the influence of the dense environments of galaxy clusters (e.g. Amram et al. 1996 and references therein).

Our results on several CGGs have already been published: (1) the "Cartwheel" compact group, a quartet of galaxies containing the well-known ring galaxy called the "Cartwheel galaxy" produced by the encounter of a small galaxy intruder through the spin axis of a large target galaxy (Amram et al. 1998); (2) HCG 16, one of the most dense compact groups known where a major merger event has taken place; this group could be a young compact group in formation

Send offprint requests to: P. Amram,
e-mail: Philippe.Amram@oamp.fr

⋆ Based on observations collected at the European Southern Observatory, La Silla, Chile and at the Canada-France-Hawaii Observatory, Hawaii, USA.

⋆⋆ Tables 1 and 2, Figs. 1, 3, 5, 7, 9, 11, 13, 15, 23 are only available in electronic form at http://www.edpsciences.org

through the merging of close-by objects in a dense environment (Mendes de Oliveira et al. 1998); (3) HCG 90, a dynamically evolving group where three galaxies are in interaction and will possibly merge into one single object (Plana et al. 1998); (4) HCG 18, that is not a CG but instead a large irregular galaxy with several star forming clumps (Plana et al. 2000); (5) HCG 92, the famous Stephan's Quintet where collisions among group members may have taken place and formed dwarf galaxies (Plana et al. 1999; Mendes de Oliveira et al. 2001).

We present here a new data set for five Hickson compact groups. We could derive kinematic information mainly for the late-type members. We also present a comparison of rotation curves (RCs) we derived, with previous studies using long-slit spectroscopy made by Rubin et al. (1991) (hereafter referred to as RHF1991) and Nishiura et al. (2000) (hereafter referred to as NSOMT2000).

A new set of Fabry Perot observations of three Hickson Compact Groups: HCG 88, HCG 89 and HCG 100, for which we detect warm gas in 15 group members, is presented in Plana et al. (2003). In a following paper the properties of the CGGs will be compared to those of an homogeneous sample of nearby isolated spirals with a large range of morphological types and luminosities for which Fabry-Perot data are also available, allowing statistical studies: the GHASP[1] survey (Amram & Garrido 2002; Garrido et al. 2002, 2003).

2. Observations

Observations were carried out during two runs at the European Southern Observatory 3.6 m telescope (ESO 3.6 m) in August 1995 and at the Canada-France-Hawaii 3.6 m telescope (CFHT 3.6 m) in August 1996.

During the run at the ESO 3.6 m telescope, the Fabry Perot instrument CIGALE was used. It is composed of a focal reducer (bringing the original f/8 focal ratio of the Cassegrain focus to f/2), a scanning Fabry-Perot and an Image Photon Counting System (IPCS). The IPCS, with a time sampling of 1/50 s and zero readout noise, makes it possible to scan the interferometer rapidly (typically 5 s per channel), avoiding sky transparency, air-mass and seeing variation problems during the exposures.

At the CFHT 3.6 m, the multi-object spectrograph focal reducer (MOS), attached to the f/8 Cassegrain focus, was used in the Fabry-Perot mode. The CCD was a STIS 2 detector, 2048×2048 pixels with a read-out noise of 9.3 e^- and a pixel size on the sky of 0.86 arcsec after 2×2 binning to increase the signal to noise ratio.

Tables 1 and 2 contain the journal of observations and observational characteristics for both runs. Reduction of the data cubes were performed using the CIGALE/ADHOC software (Boulesteix 2002). The data reduction procedure has been extensively described (Amram et al. 1998 and references therein).

Wavelength calibration was obtained by scanning the narrow Ne 6599 Å line under the same conditions as the observations. Velocities measured relative to the systemic velocity are very accurate, with an error of a fraction of a channel width (<3 km s^{-1}) over the whole field.

Subtraction of bias, flat fielding of the data and cosmic-ray removal have been performed for each image of the data cube for the CFHT observations. To minimize seeing variation, each scan image was smoothed with a gaussian function of full-width at half maximum equal to the worse-seeing data of the data cube. Transparency and sky foreground fluctuations have also been corrected using field star fluxes and galaxy-free windows for the CFHT observations. Except for flat fielding, none of these operations are necessary for the IPCS data processing (ESO observations).

The signal measured along the scanning sequence was separated into two parts: (1) an almost constant level produced by the continuum light in a narrow passband around Hα (hereafter referred to as continuum map) and (2) a varying part produced by the Hα line (hereafter referred to as Hα emission line map *or* monochromatic map). The continuum level was taken to be the mean of the three faintest channels, to avoid channel noise effects. The Hα integrated flux map was obtained by integrating the monochromatic profile in each pixel. The continuum as well the Hα images are not flux calibrate due to a lack of useful calibrators; hence, the contour plots are given in arbitrary units. The velocity sampling was 11 km s^{-1} at CFHT and 16 km s^{-1} at ESO. Profiles were spatially binned to 3×3 or 5×5 pixels in the outer parts, in order to increase the signal-to-noise ratio. Strong OH night sky lines passing through the filters were subtracted by determining the level of emission from extended regions away from the galaxies (Laval et al. 1987).

3. Description of the groups

In this section, we describe the main characteristics of all the galaxies observed in each group. Table 3 summarizes the general properties of the observed galaxies and Table 4 gives the different galaxy position angles, inclination and maximum rotation velocity that we derived from the continuum, monochromatic and velocity maps. Figures 1, 3, 5, 7, 9, 11, 13, 15, 18 and 23 show the different maps (continuum, monochromatic and velocity). Figures 2, 4, 6, 8, 10, 12, 14, 17, 19, 21, 22, 24, 25, 26 and 27 display the different rotation curves (RCs) for each group member and, when available, comparison with other authors' data (Figs. 14, 17 and 25). Figure 20 shows line profiles and different maps (continuum, monochromatic and velocity for the two components of the galaxy). A Hubble constant $H_0 = 75$ km s^{-1} Mpc^{-1} is used throughout this paper.

3.1. HCG 10

This group is formed of four members, three are late-type objects (SBb, Sc and Scd) and one is an elliptical galaxy (E1). A multiphase interstellar medium has been detected in this group. Only the two galaxies with the latest morphological types, HCG 10a and c, have been detected at 60 and 100 μm (IRAS data), suggesting the presence of dust (Allam et al. 1996). In order to calculate the HI deficiency of the group, its HI content has been taken as the sum of the HI content of the

[1] http://www.oamp.fr/interferometrie/ghasp/ghasp.html

Table 3. Properties of HCG members.

(1)	(2)	(3)	(4)	(5)	(6)	(7)	(8)	(9)	(10)
	Name	α	δ	T	$V_{\rm Syst}$	D	$B_{\rm Tc}$	$D_{25}/2$	
		1950	1950		km s^{-1}	Mpc	mag	$''$	kpc
HCG 10 a	NGC 536	01h 23m 31.0s	34°26′33.3″	SBb	5148	66.0	12.62	44	14.1
c	NGC 531	01h 23m 28.4s	34°29′40.1″	Sc	4660	66.0	14.07	28	9.0
d	NGC 542	01h 23m 40.4s	34°24′56.5″	Scd	4620	66.0	14.69	29	9.3
HCG 19 a	MCG -02-07-073	02h 40m 14.3s	−12°38′00.4″	E2	4279	54.2	14.00	36	9.5
b	MCG -02-07-074	02h 40m 18.0s	−12°36′23.6″	Scd	4210	54.2	15.42	28	7.4
c	MCG -02-07-075	02h 40m 22.7s	−12°39′35.6″	Sdm	4353	54.2	14.46	39	10.2
HCG 87 a	ESO 597- G 036	20h 45m 23.0s	−20°02′05.3″	Sbc	8694	117.7	13.97	47	26.8
c	ESO 597- G 035	20h 45m 20.2s	−20°01′02.1″	Sd	8920	117.7	15.02	21	12.0
HCG 91 a	NGC 7214	22h 06m 17.2s	−28°03′19.9″	SBc	6832	93.6	12.62	65	29.5
c	ESO 467- G 013	22h 06m 23.7s	−28°01′41.4″	Sc	7319	93.6	14.47	26	11.8
HCG 96 a	NGC 7674	23h 25m 24.6s	+08°30′09.9″	Sc	8698	117.2	13.53	33	18.8
c	NGC 7674A	23h 25m 26.5s	+08°30′26.4″	Sa	8753	117.2	15.69	6	3.4
d	PGC 071507	23h 25m 27.9s	+08°29′30.7″	Im	8975	117.2	16.56	–	–

Description of the columns: (1) Identification from Hickson (1993); (2) Alternative identification; (3) Right ascension (1950) from Hickson (1993); (4) Declination (1950) from Hickson (1993); (5) Morphological type, from Hickson (1993); (6) Systemic velocity from Hickson (1993), except for HCG 19c coming from NED; (7) Distance of the group. The distance has been computed from the mean redshift of the group extracted from Table 3 of Hickson et al. (1992). A Hubble constant of $H_0 = 75$ km s^{-1} Mpc^{-1} has been used. To derive the distance we have used the method described in Paturel et al. (1997), i.e. the velocity of the group has been corrected to the centroid of the Local Group and for infall of the Local Group towards Virgo using an infall velocity of 170 km s^{-1}; (8) Asymptotic magnitude corrected for internal and external extinction, from Hickson (1993); (9) Optical radius in arcsec, from NED; (10) Optical radius in kpc, using Cols. (7) and (9).

individual galaxies (Verdes-Montenegro et al. 2001). HCG 10 is among the less HI deficient ($Def_{\rm HI} = 0.24$) HCGs according to Verdes-Montenegro et al. (2001), who found an average value of $Def_{\rm HI} = 0.36$ for their sample of 72 HCGs. Another component of the cold ISM, the CO emission, has been detected only for HCG 10a and 10c. Leon et al. (1998) computed a mean star formation efficiency (SFE) for their sample of compact groups ($\mathrm{Log}(L_{\rm FIR}/M_{\rm H_2}) = 0.39$), showing that the compact environment has a moderate effect on triggering global star formation. For HCG 10a and 10c the SFE is lower than the average SFE for their sample ($\mathrm{Log}(L_{\rm FIR}/M_{\rm H_2}) = -0.63$ and 0.14 respectively). HCG 10 has been detected as a faint X-ray emitter by Ponman et al. (1996) using ROSAT data. HCG 10b, the elliptical galaxy of the group, for which Pildis et al. (1995) pointed out a shell structure surrounding the whole galaxy, was not observed in our program, being too far (9 arcmin) from the group center (the FOV of the instrument is 7.3 arcmin). HCG 10a has been classified as an AGN (Shimada et al. 2000). We obtained velocity, monochromatic and continuum maps for 10a, 10c and 10d.

The SBb galaxy HCG 10a has a bright inner region, a ring from which two faint arms emanate and a very weak level of Hα emission. Shimada et al. (2000) did not detect Hα line emission in HCG 10a. Both arms are visible on the continuum image and are traced by the HII regions detected in the galaxy. Indeed, the emission lines surrounding the centre of the galaxy are suspicious because the continuum emission is very bright and the signal which could possibly be from Hα emission around the nucleus matches the intensity level of the continuum photon noise. The values of the velocities provided by this central emission are also highly doubtful. As a consequence of the weakness of the Hα emission, the Hα velocity determination is uncertain. A RC as uncertain as the velocity field has been plotted, using the morphological parameters. This RC is shown only to indicate the velocity range of the galaxy and should not be used for further discussion.

HCG 10 c and d show clumpy emission gas distributions. For HCG 10c, the signature of the spiral-arm structure is clearly seen in the DSS or the *R*-band image (not presented) as well as in the velocity field, where wiggles on the isovelocity contours are visible. Two bright Hα knots are clearly superimposed on the wiggles of the isovelocity contours of HCG 10c. A spiral structure is also seen, although less obvious, on the isovelocity contours of HCG 10d. The *R*-band image as well as the continuum image of HCG 10c exhibit a strong nucleus and the brightest central HII region presents an offset of 2.6 arcsec with respect to the nucleus (defined as the pixel position of the maximum central emission from the continuum map). In the continuum image, HCG 10c also shows two very weak and diffuse extensions (in the northeast and southwest), which could suggest the presence of a warped disk or, alternatively, distorted spiral arms. These diffuse extensions are oriented along the direction of the stellar major axis (33°), as deduced from the continuum images. In contrast, the gaseous velocity field indicates that the position angle (hereafter referred to as PA) of the major axis is oriented northwest-southeast (153°), meaning that the stellar and the gaseous kinematics are decoupled. The velocity field is not regular and the PA of the gaseous major axis we determined

Table 4. Kinematic properties of the HCG members.

Name	Position Angle (degrees)			Inclination (degrees)			Maximum Rotation Velocity (km s^{-1})
	Velocity map	Cont. map	Mono. map	Velocity map	Cont. map	Mono. map	Approaching / Receding side
HCG 10 a	–[a]	80 ± 5	–[a]	–[a]	74 ± 5	–[a]	−200 / +175
c	153 ± 3	33 ± 8	145 ± 10	48 ± 5	64 ± 5	60 ± 10	−151 / +150
d	147 ± 8	135 ± 10	135 ± 5	68±5	75 ± 3	72 ± 5	−141 / +150
HCG 19 a	67 ± 10	44 ± 8	80 ± 15	53 ± 10	57 ± 3	44 ± 5	−120 / +180
b	90 ± 5	87 ± 15	93 ± 13	60 ± 10	35 ± 3	52 ± 5	−117 / +74
c	103 ± 5	105 ± 8	92 ± 6	55 ± 10	50 ± 3	55 ± 5	−107 / +124
HCG 87 a	52 ± 10	50 ± 10	50 ± 10	85 ± 10	70 ± 10	73 ± 3	−208 / +191
c	82 ± 3	90 ± 1	90 ± 4	50 ± 3	60 ± 3	64 ± 5	−197 / +166
HCG 91 a	0 ± 3	50 ± 50[b]	55 ± 10[b]	50 ± 3	50 ± 5[b]	55 ± 10[b]	−294 / +336
c1	141 ± 2	125 ± 10	100 ± 10	40 ± 5	50 ± 5	31 ± 10	−112 / +111
c2	125 ± 2	125 ± 5	120 ± 10	45 ± 5	50 ± 5	60 ± 10	−130 / +100
HCG 96 a	132 ± 5	150 ± 10	135 ± 20	50 ± 5	60 ±?	60 ± 5	−259 / +107
c	33±	33 ± 5	33 ± 5	57 ± 5	53 ± 3	60 ± 5	−111 / +80
d	10 ± 8	0 ± 3	25 ± 15	48 ± 3	56 ± 3	57 ± 5	−62 / +43

[a] It was not possible to measure this angle.
[b] The measurement was done after masking the southern tidal arm.

is an average value for the whole field. The isovelocities present an U-shape with respect to the gaseous position angle and not an S-shape, as expected for a warp structure. Moreover, the distortions are probably not due to a warp of the disk, since the stellar and gaseous PAs are significantly different and a warp of the disk should follow the stellar distribution rather than the gaseous matter. In conclusion, the faint structures measured in the *R*-image or in the continuum map are more likely extensions of the spiral arms rather than a warp. The RC of HCG 10c shows a linear shape and extends up to 24 arcsec (7.7 kpc), almost reaching the optical radius ($D_{25}/2$ = 28 arcsec = 9 kpc) for a velocity of 170 km s^{-1}. Since the continuum image of this galaxy shows a bright central region, the linear shape of the RC will probably make it difficult to reconcile with a reasonable *M/L* value for the stellar disk and imposes the need for a strong dark-matter component. The bumps around 14 arcsec (4.5 kpc) on both sides of the RC are due to the crossing of the spiral arms; the bump is stronger for the receding side, consistent with the velocity field.

The velocity field of HCG 10d is rather regular and both stellar and gaseous major axes are aligned. The RC of HCG 10d is also quite regular and reaches almost the optical radius ($D_{25}/2$ = 29 arcsec = 9.3 kpc) at a rotation velocity of 150 km s^{-1}. The approaching side does not extend as far as the receding side. This could be due to the fact that the edge of the approaching side was placed on the edge of the receptor and of the interference filter.

3.2. HCG 19

Hickson (1993) originally catalogued four members in this group, but HCG 19d was later found to be a background object, with a velocity of over 20000 km s^{-1} (de Carvalho et al. 1997). The triplet contains two late-type spirals (Scd and Sdm) and one elliptical galaxy (E2). The two spiral galaxies show signs of morphological distortions. HCG 19 has been detected in FIR at 60 and 100 μm. HCG 19b is the brightest FIR source of the group, while for the other two members, only upper limits on the detection are provided from IRAS data (Allam et al. 1996). In contrast with HCG 10, the HI component detected by Verdes-Montenegro et al. (2001) for HCG 19 shows a HI gas deficiency ($Def_{\rm HI}$ = 0.58), a value which is higher than the mean derived for their whole sample ($Def_{\rm HI}$ = 0.36). CO emission has been detected for HCG 19b only (Leon et al. 1998). HCG 19b shows the highest SFE for their sample of compact groups (Log($L_{\rm FIR}/M_{\rm H_2}$) = 0.86), the mean value being Log($L_{\rm FIR}/M_{\rm H_2}$) = 0.39. This group does not present diffuse X-ray emission (Ponman et al 1996).

HCG 19a shows a very weak Hα emission but rather extended for an elliptical galaxy. The brightest HII region is slightly offseted from the nucleus of the galaxy by 2 arcsec (0.5 kpc). The PAs of the major axes of the stellar and gaseous components differ by 23°. HCG 19a has a rather regular velocity field for an elliptical and its RC displays an important circular rotation with a maximum at 120 km s^{-1}, for the receding side and 180 km s^{-1}, for the approaching side. The irregularities in the velocity field of HCG 19a are partly due to the weak S/N in the Hα profiles. Nevertheless, four main characteristics can be noted: (1) The RC almost reaches the optical radius ($D_{25}/2$ = 36 arcsec = 9.5 kpc), which is actually uncommon for gaseous components in elliptical galaxies; (2) in the central regions, within 8 arcsec (2.1 kpc), the isovelocities are strongly distorted due to the offset of the brightest Hα knot with respect to the stellar nucleus; this induces a flat inner RC for the

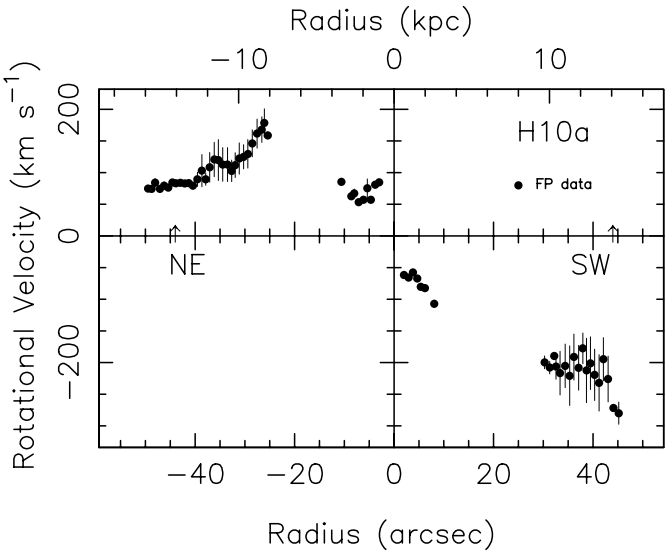

Fig. 2. Generic caption for Figs. 2, 4, 6, 8, 10, 12, 14, 17, 19, 21, 22, 24, 25, 26 and 27: rotation curve of the galaxy, each side is represented by a different symbol only when one quadrant is displayed. The error bars give the dispersion in each circular annulus. The arrow along the *x*-axis indicates the optical radius ($D_{25}/2$, from RC3 catalog), when this distance fits in the range of the plot. HCG 10a is plotted here.

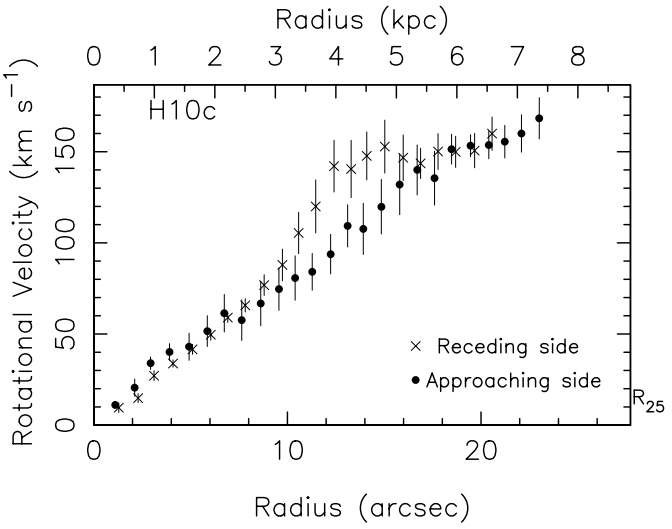

Fig. 4. HCG 10c: same as Fig. 2.

receding side; (3) both sides of the RC are decreasing after a certain radius (20 arcsec, which corresponds to 5.3 kpc, for the approaching side and 28 arcsec, which corresponds to 7.4 kpc, for the receding side); (4) whatever kinematic parameters we may impose, we cannot make both sides of the RC match.

HCG 19b is a very faint and diffuse Scd galaxy (Hickson 1993) or (R)SB(r)a pec (NED[2]), as can been seen from the DSS image and from the continuum image. The nucleus of the galaxy is shifted by 2 arcsec (0.5 kpc) to the east with respect to the very bright central Hα knot. The velocity field is patchy but leads to a symmetric RC up to 29 arcsec (7.6 kpc). Further out, the approaching side keeps rising up to 42 arcsec (11 kpc) while the receding side decreases up to 46 arcsec (12.1 kpc). An isolated HII region is responsible for a sharp rise of the velocities in the outer region of the approaching side while the decreasing trend of the receding side is traced by diffuse Hα emission. The distorted shape of the velocity field could be due to a warp, since the galaxy is rather inclined (60°). However, one cannot be sure of the presence of such a warp because we do not observe a symmetric S-shape in the velocity field – thus, we cannot exclude that streaming motions could be induced by interaction of this galaxy with the other members of the group.

HCG 19c is a Sdm galaxy (Hickson 1993) or a SBm pec (NED), which shows amorphous arms both in the continuum and in the monochromatic maps but with a regular velocity field and RC. The PA of the major axes of the stellar and gaseous disks differ by 8°. The Hα distribution is non axisymmetric. Furthermore, an outer and extended region towards HCG 19a (to the west) is visible in the Hα distribution as well as in the velocity field. This western, extended and approaching region induces, on one side of the RC, very low rotation velocities at radii larger than 18 arcsec (4.7 kpc). In the central regions (within 10 arcsec or 2.6 kpc), the agreement between both sides is very good while at intermediate radii (between 10 and 18 arcsec which corresponds to 2.6 and 4.7 kpc) the approaching side has velocities typically 20 km s^{-1} lower than that the ones of receding side. On the other hand, at very low intensity levels (~2−3 σ above the rms noise), a second Hα component is superimposed from 10 to 22 arcsec (2.6 to 5.8 kpc), making the link between the intermediate disk and the outer western region. In conclusion, the external western region could represent an extension of a distorted main disk and a signature of an interaction with the neighbor HCG 19a.

3.3. HCG 87

This group is a small compact system composed of a triplet of galaxies (a, b and c) with a background galaxy superimposed onto it (HCG 87d). HCG 87a is a large edge-on Sbc spiral galaxy showing a strong dust lane. HCG 87c is a late-type galaxy (Sd) and HCG 87b is an S0 or an elliptical galaxy showing no Hα emission. An HST image of the group taken with the WFPC2 (English et al. 1999) provides a striking improvement in resolution over previous ground-based imaging. In particular, this image reveals complex details in the dust lanes of the group's largest galaxy member (HCG 87a), which is actually disk-shaped, but tilted (isophotal warping); moreover the thick disk is asymmetric radially as well as in the *z*-direction. In addition, a faint tidal bridge of stars can be seen between the edge-on galaxy and the early-type galaxy. Both HCG 87a and b have active galactic nuclei (Shimada et al. 2000) in their centers. The third group member, the nuclear starburst spiral galaxy, may be undergoing a burst of active star formation (Coziol et al. 1998). Indeed, gravitational tidal forces between interacting galaxies can provide fresh fuel for both active nuclei and starburst phenomena by intensifying gas flows toward the center of HCG 87a. Only a lower limit

[2] NASA/IPAC Extragalactic Database.

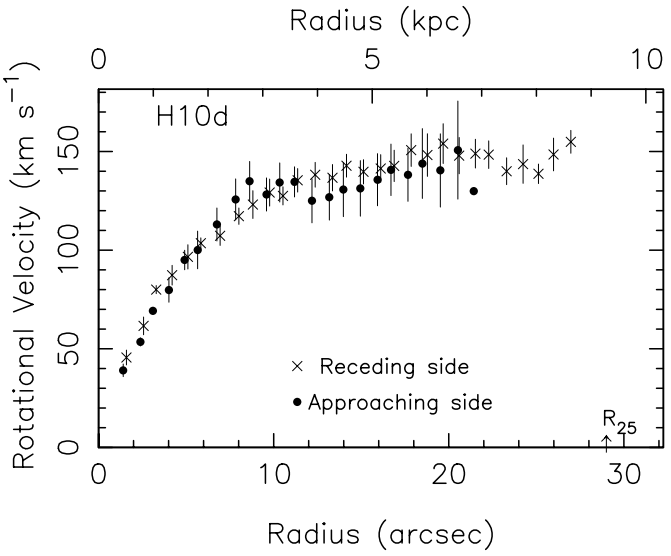

Fig. 6. HCG 10d: same as Fig. 2.

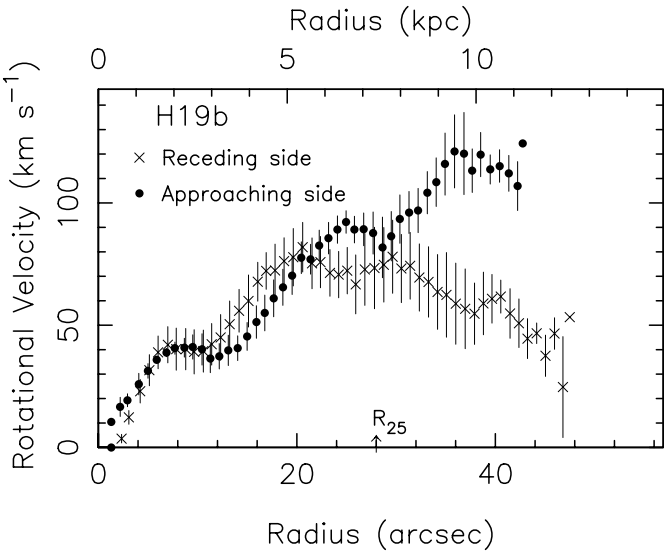

Fig. 10. HCG 19b: same as Fig. 2.

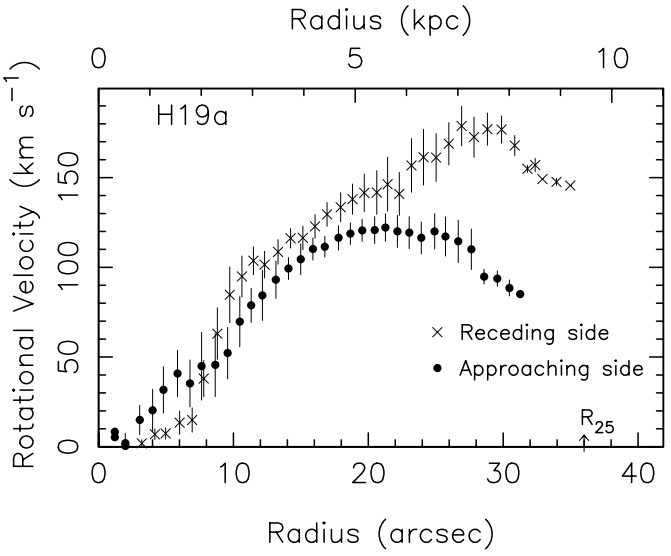

Fig. 8. HCG 19a: same as Fig. 2.

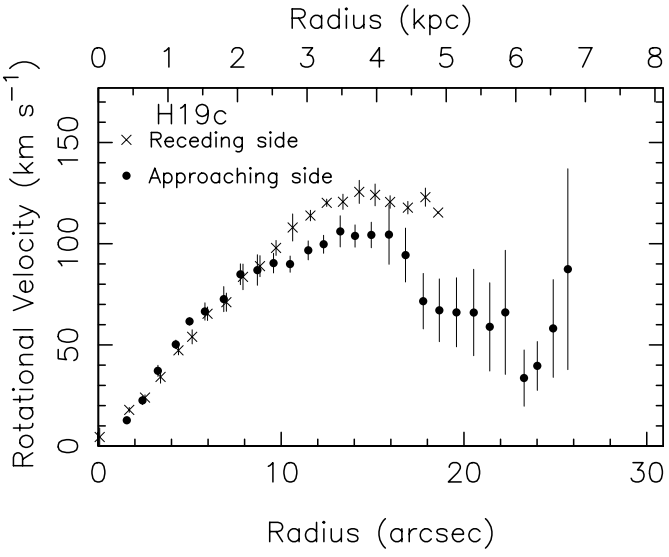

Fig. 12. HCG 19c: same as Fig. 2.

of 0.46 K km s^{-1} has been provided for the CO content of HCG 87a (Boselli et al. 1996). No FIR emission has been reported by IRAS (Allam et al. 1996). Ponman et al. (1996), using ROSAT data, gave upper limits for the X-ray luminosity of the group (Log L_X < 42.36 erg s^{-1})[3]. Verdes-Montenegro et al. (2001) showed that this group has a high HI deficiency ($Def_{HI} = 0.88$). The morphological type of the large edge-on and dusty galaxy HCG 87a is uncertain. It was classified by Hickson (1993) as an Sbc, by Milhos et al. (1995) as an S0 and by NED as an S0 0 pec sp. A peanut-shape bulge, boxy and with strong X-feature, like HCG 87a, (Shaw et al. 1990; Jarvis 1986) can be reproduced in simulations from secular evolution for an S0 galaxy (Mihos et al. 1995).

We obtained Hα and velocity maps for HCG 87a and HCG 87c and for HCG 87b we could not detect any Hα emission. The emission of HCG 87a is concentrated on the northeastern half of the galaxy. On the HST image, it can been seen that the dust lane is more compact and opaque on the southwestern side of the galaxy (absorbing the Hα and [NII] emission line) than on the northeastern one.

The monochromatic map of HCG 87a shows four fairly intense (for an early-type galaxy) Hα knots, the brightest being close to the center of the galaxy. HCG 87a is nearly edge-on, but probably not exactly edge-on ($i = 85° \pm 5°$), since the disk appears thicker on the northern side of the dust lane than on the southern side. The linear shape of the RC leads to the conclusion that the disk is in solid-body rotation, as already reported by Burreau & Freeman (1999) and NSOMT2000. Nevertheless, the high inclination of the galaxy probably strongly affects the shape of the RC by inducing beam-smearing effects. The RC reaches 70% of the optical radius ($D_{25}/2$ = 48 arcsec or 27.4 kpc), which is fairly extended if the galaxy is actually an S0, but probably insufficient to

[3] Ponman et al. (1996) have used H_0 = 50 km s^{-1} Mpc^{-1}; in the present paper we use H_0 = 75 km s^{-1} Mpc^{-1}.

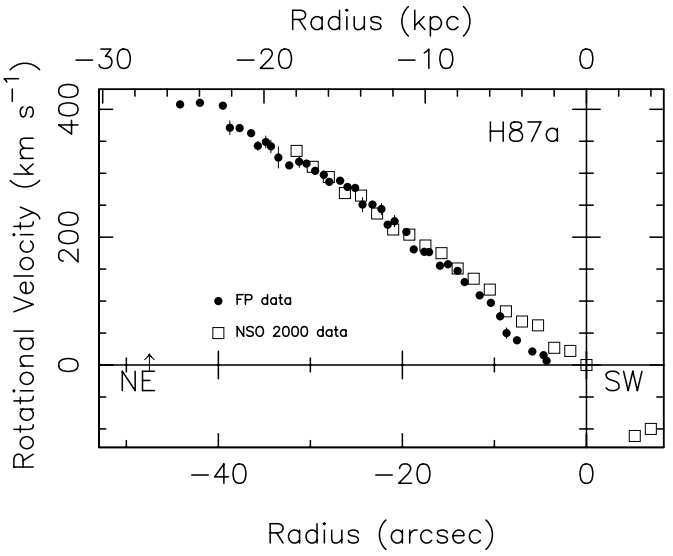

Fig. 14. HCG 87a: rotation curves using our data and NSOMT2000. The kinematic parameters used to plot the RCs are, for the inclination, 85° and 90° respectively, and for the position angle of the major axis, 52° and 56° respectively.

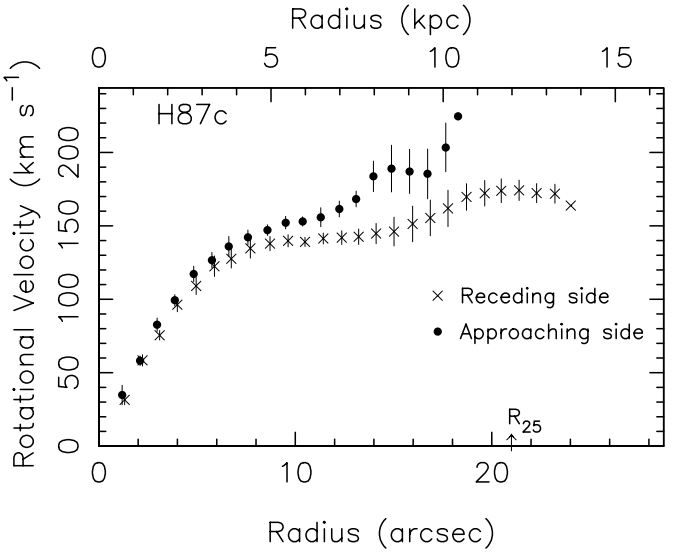

Fig. 16. HCG 87c: same as Fig. 2.

reach the plateau of the RC. Furthermore, an early-type, massive galaxy, with an extended gas disk, is not expected to have a solid body RC, arguing in favor of a curve strongly affected by absorption effects. The agreement between NSOMT2000 and our data is good, except for small radii. A comparison with the data from Burreau & Freeman (1999) also shows good agreement. In summary, the RC of HCG 87a is truncated on one side, most probably because of the strong dust lane in the south-western side of the galaxy. However, we cannot disentangle the effects of absorption, secular evolution and environment in the RC of HCG 87a.

The monochromatic map of HCG 87c shows bipolar HII structures, where the brightest one corresponds almost exactly to the nucleus of the galaxy. The velocity field and the RC clearly exhibit an asymmetry on both sides of the galaxy for

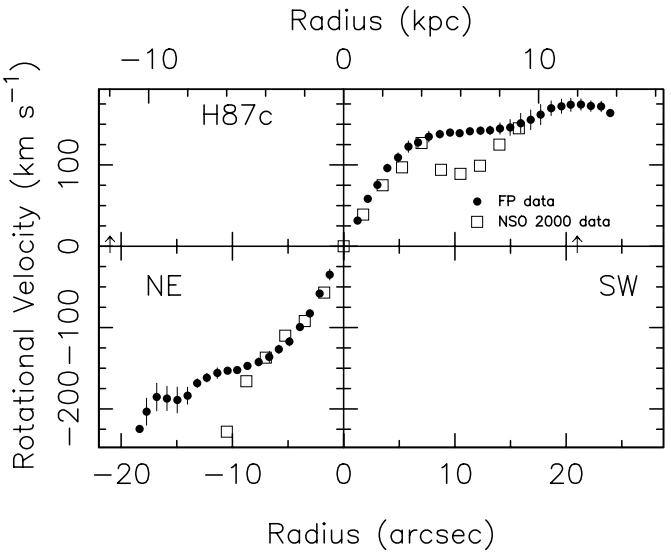

Fig. 17. HCG 87c: RCS using our data and NSOMT2000 data. The kinematic parameters used to plot the RCs are, for the inclination, 50° and 76° respectively and for the position angle of the major axis, 82° and 90° respectively.

radii larger than 8 arcsec (4.6 kpc). Whatever the kinematic parameters are, both sides of the RC cannot match at all radii. The shape of the velocity field indicates that this asymmetry could be the result of a warp of the disk or elliptical distortions in a planar disk. We compare our RC with that obtained by NSOMT2000. Despite our disagreement on the inclination (52° measured by us and 76° by them) both curves match within 7 arcsec (4 kpc). At larger radii, the RCs strongly diverge, the curve derived by us being more regular and extended than that derived by NSOMT2000. However, the RC we obtain is not symmetric, which could be due to interactions with one or more companions in the group.

3.4. HCG 91

This quartet of galaxies (also known as VV 700) is formed by four late-type galaxies, two of which are barred: HCG 91a and d (Hickson 1993). A faint double tidal tail can be seen between HCG 91a and HCG 91c, from the DSS image of the group. Allam et al. (1996) reported 60 μ and 100 μ emission for HCG 91a and HCG 91d together. No CO detection has been reported in the literature for this group. Ebeling et al. (1994) detected point-like emission with ROSAT in the position of the group. Verdes-Montenegro et al. (2001) reported an HI deficiency $Def_{\rm HI}$ = 0.24; this value is a bit lower than the mean value for their whole sample. Barnes & Webster (2001) made a detailed study of this group in HI: the neutral gas distribution presents two knots centered around HCG 91a and HCG 91c and at lower intensity levels a connection between the two members of the group is present. Their line-of-sight velocity curves suggest that there may be a connection between the two galaxies through a gas bridge, since there is a common velocity in the southern part of HCG 91c and the northern part of HCG 91a. Roughly measured from their maps, we find that the velocity amplitudes of HCG 91a and HCG 91c are 400 km s^{-1} and

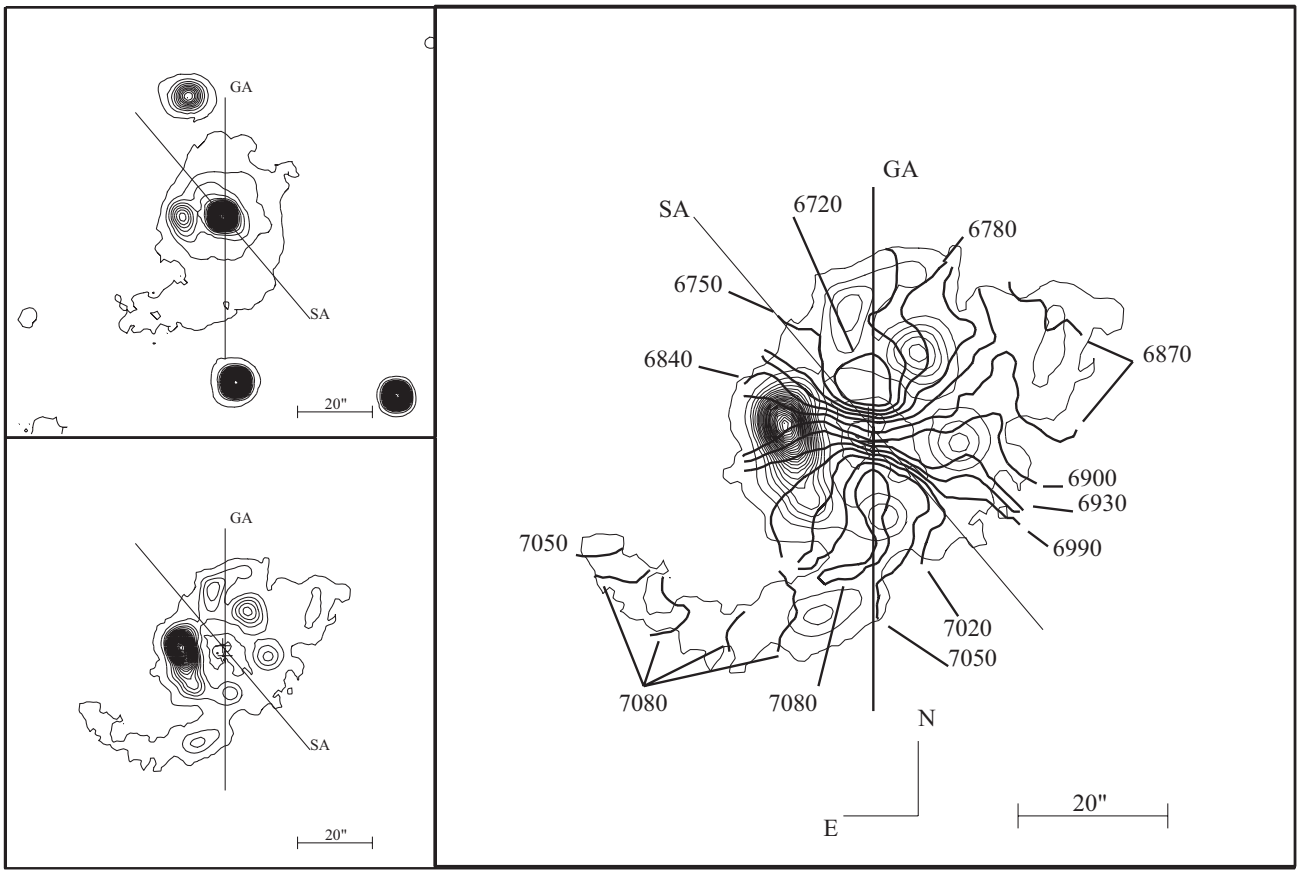

Fig. 18. HCG 91a Generic caption for Figs. 1, 3, 5, 7, 9, 11, 13, 15, 18 and 23: **(Top)** the upper left panel represents the continuum map (see text for details) onto which the stellar axis (SA) and the axis determined from the monochromatic map (GA) are superimposed . The SA is obtained by fitting the external isophotes of the continuum image. The lower left panel is the monochromatic map onto which the same axes (SA and GA) are plotted. The right panel shows the velocity field (in bold) superimposed onto the monochromatic map. SA and GA are also plotted here. The kinematic center is represented by a cross.

140 km s^{-1} respectively which is roughly in agreement with what we find. In this study, we could derive maps for HCG 91a and HCG 91c only. We did not detect any emission for the barred galaxy HCG 91d (SB0) and HCG 91b (Sc) was out of the field of view of the instrument.

The monochromatic map of HCG 91a shows a clumpy and irregular Hα distribution. In particular, it shows an intense region to the east of the galaxy and a southern arm which, at large radii, points towards HCG 91c. A weak Hα emission superimposed onto a strong continuum is observed in the center of the galaxy. The signature of the bar (SBc) is visible along the minor axis of the velocity field while a twist of the isovelocities in the outer regions indicate a rotation of the PA. The southern spiral arm displays a roughly constant velocity, which could be a signature of streaming motions due to the interaction with HCG 91c. Both sides of the RC of HCG 91a match, from the center up to 25 arcsec (11.3 kpc) and then diverge for larger radii, with the receding side rising by about 150 km s^{-1} and the approaching side decreasing by about 130 km s^{-1}. The behavior of the RC, when both sides diverge, is probably due to streaming motions in the arms. This is more obvious for the receding side, where the tidal arm points towards HCG 91c. For the approaching side, one cannot observe any tidal arm directly on the Hα image (even if a diffuse pattern is visible on the DSS and the Hα images), but the perturbation in the velocity field where the RC diverges could be the kinematic signature of a symmetric northern tidal arm.

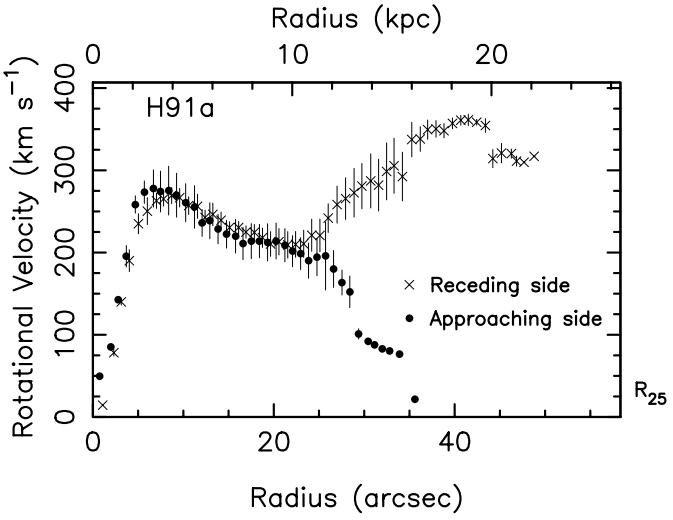

Fig. 19. HCG 91a: same as Fig. 2.

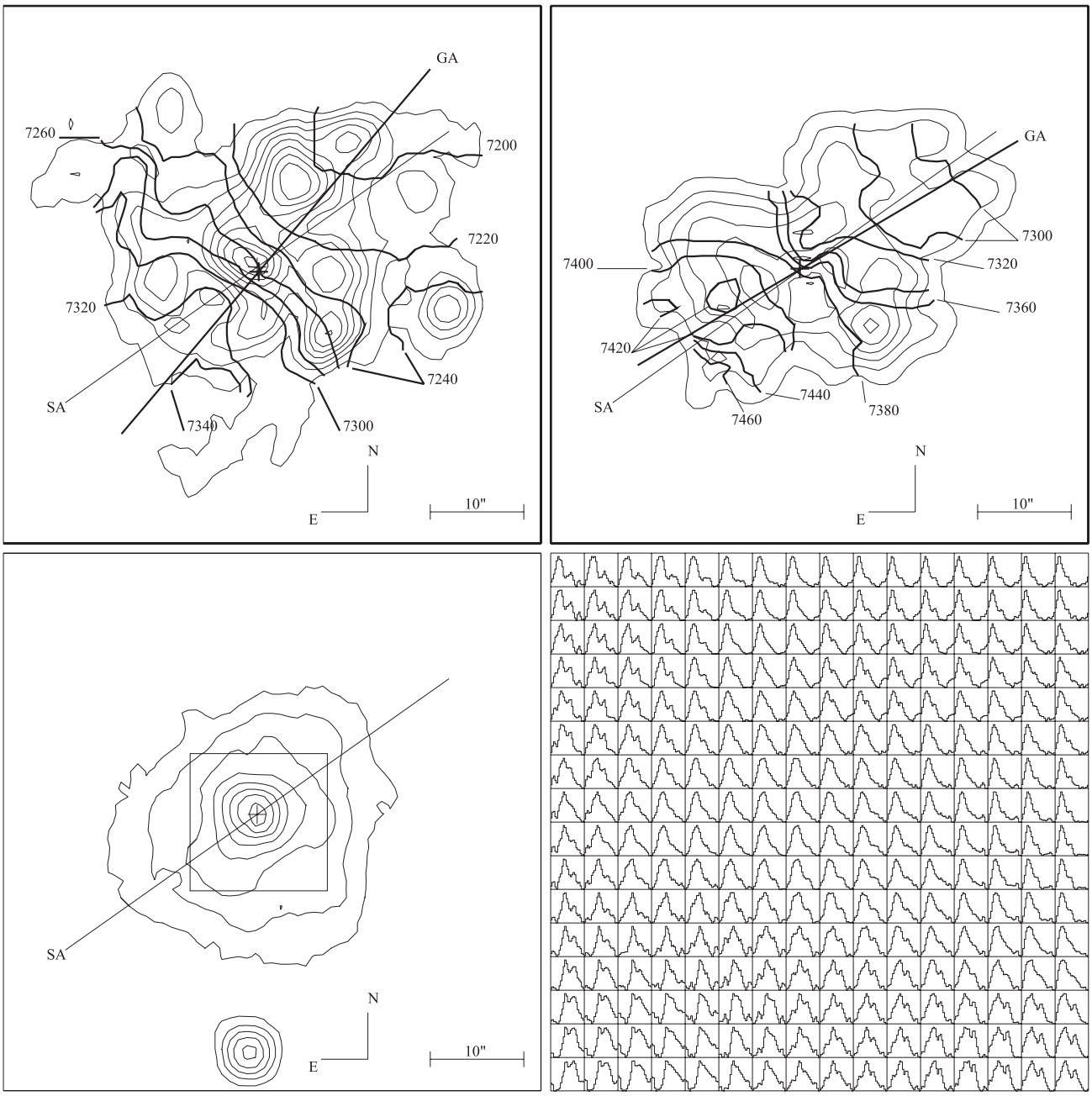

Fig. 20. HCG 91c: **Upper left panel**: main gas component velocity field superimposed onto the monochromatic map. **Upper right panel**: velocity field and monochromatic map for the second gas component. **Bottom left panel**: continuum map; the square in the central region represents the region enlarged in the bottom right panel. **Bottom right panel**: profiles in the center of HCG 91c. Each pixel represents 0.91 arcsec on the sky (0.4 kpc) and the *x*-axis range displays the free spectral range of 378 km s^{-1}, starting from 7157 km s^{-1} (channel 1, 6719.5 Å) up to 7535 km s^{-1} (channel 24, 6727.8 Å). Each profile was arbitrary normalized to fit the box size (*y*-axis).

HCG 91c presents two gas components, which could be detected in the central profiles of the galaxy, as it can be seen from the double components in the profiles. The extension of the main gas component is a bit larger than that of the second component. The major-axis PAs of the components are similar. Both components are also rotating in the same sense. Their monochromatic maps appear to be clumpy and the velocity fields are quite regular. Their RCs have good agreements between the receding and approaching sides even if the RC of the first component is not as symmetric as that for the second component. Both velocity maps show variations of the PA with respect to the radius.

3.5. HCG 96

This group, also known as Arp 182 and VV 343, shows a bright spiral galaxy (HCG 96a) with a close companion (HCG 96c). These two members appear to be strong IR emitters (Allam et al. 1996). Ponman et al. (1996) listed only an upper limit for the X-ray luminosity of this group. Leon et al. (1998)

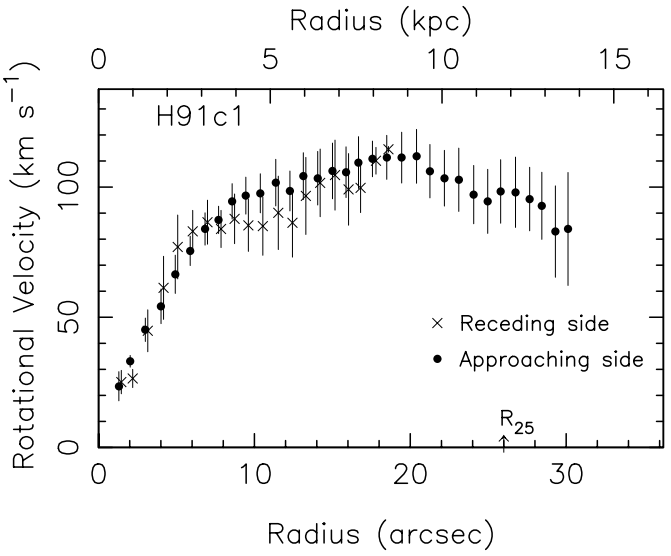

Fig. 21. HCG 91c: main component RC. Same as Fig. 2.

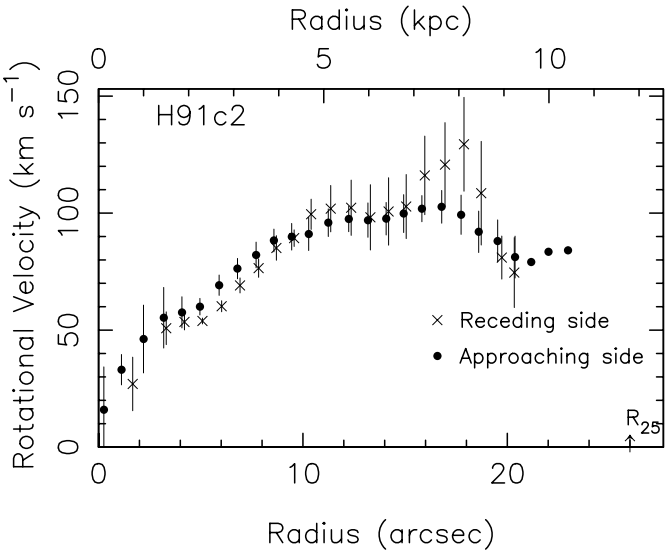

Fig. 22. HCG 91c: second component RC. Same as Fig. 2.

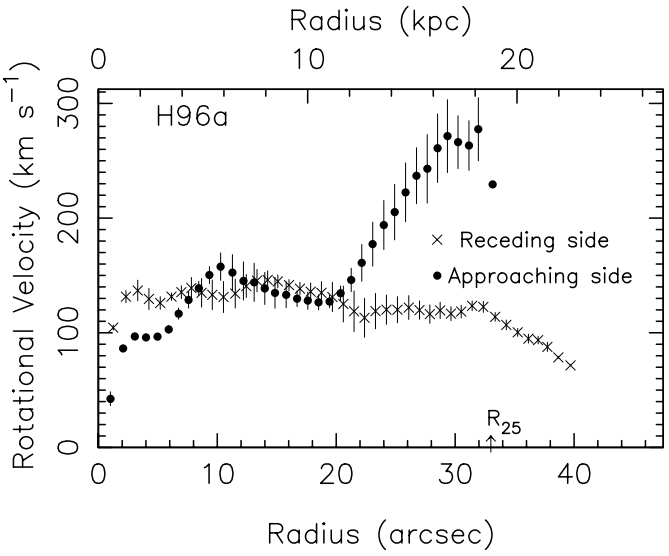

Fig. 24. HCG 96a: same as Fig. 2.

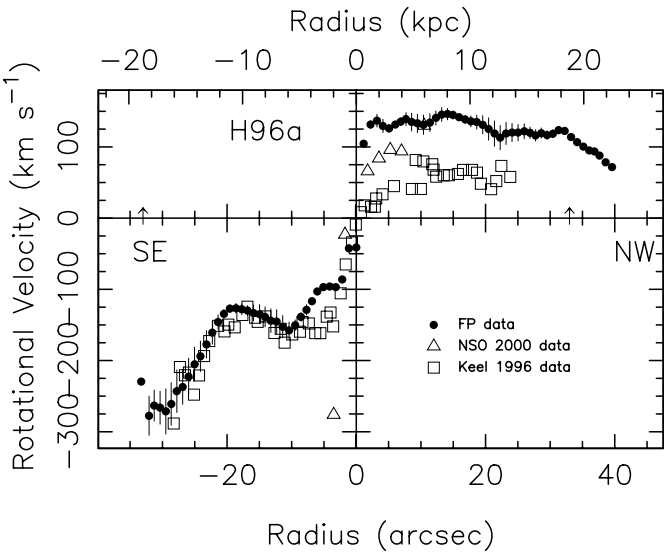

Fig. 25. HCG 96a: RCs for HCG 96a using our data, Keel et al. (1996) and NSOMT2000 data. The kinematic parameters used to plot the RCs are, for the inclination, 50°, 53° and 25° respectively and for the position angle of the major axis, 132°, 148° and 90° respectively.

detected CO emission for both HCG 96a and HCG 96c and showed that HCG 96a has an SFE above the mean SFE value for their whole sample. Verdes-Montenegro et al. (2001) found a lower limit for the HI mass of the group, leading to an HI deficiency $Def_{\rm HI}$ = 0.17. The other members of the group are a giant E2 galaxy (HCG 96b) and HCG 96d, a galaxy classified as an Im by Hickson et al. (1989). HCG 96a has been the subject of numerous publications, mainly owning to its classification as a Seyfert 2 galaxy by Mirabel & Wilson (1984). Detailed study about the nature and the activity of this galaxy can be found in Verdes-Montenegro et al. (1998) and Shimada et al. (2000). Verdes-Montenegro et al. (1997) has shown that two long low-surface brightness tails emerge from the region between H96a and c, one to the NE and the other to the NW. They also detect a shorter tail in the disk of H96a, N of its center.

Figures 11 and 12 show the velocity, monochromatic, continuum maps and the RCs for the three galaxies we observed in HCG 96 (all but HCG 96b, which has no gas). The velocity field of HCG 96a is regular in the center but highly disturbed to the southeast. The monochromatic map shows two bright emission regions, with the shape of spiral arms, consistent with the spiral arms of the galaxy. Bright emission regions can also be seen in the south and in the northwestern part of the galaxy. The continuum image shows a very peaked emission in the center and also hint the spiral pattern.

We derived a RC for HCG 96a which looks similar (in shape) to that of HCG 91a. We find a good agreement between the receding and approaching sides between radii of 10 and 20 arcsec (5.7 and 11.4 kpc), where a plateau is reached. Using the continuum center we cannot have a good agreement between receding and approaching sides in the very central part (0 to 8 arcsec or 0 to 4.5 kpc). If we, instead, move the po-

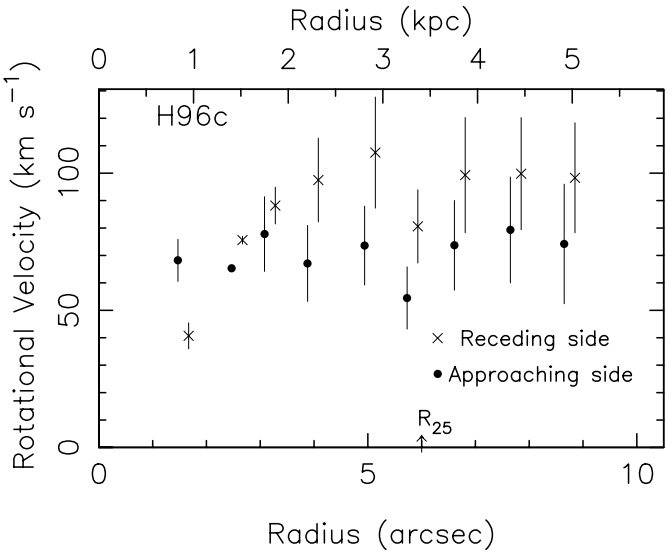

Fig. 26. HCG 96c: same as Fig. 2.

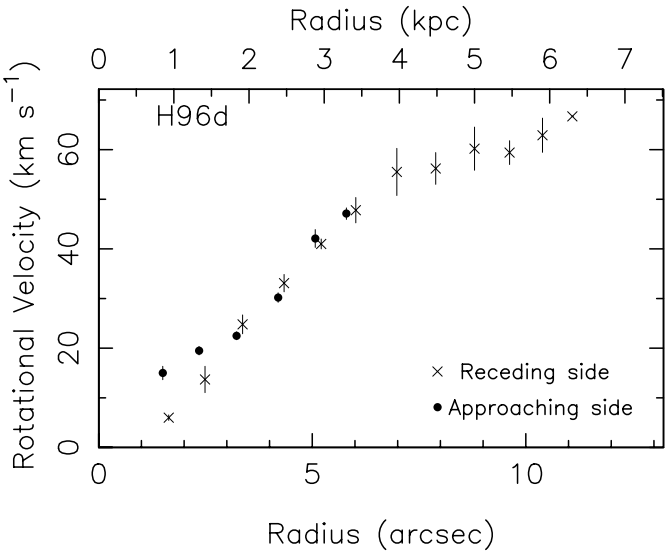

Fig. 27. HCG 96d: same as Fig. 2.

sition of the center by 2 pixels along the minor axis of the galaxy, the agreement in the inner part is much better but then, there is no agreement in the plateau region (between 10 and 20 arcsec or 5.7 and 11.4 kpc). In any case, there is a complete disagreement for radii larger than 20 arcsec (11.4 kpc), where the approaching side shows a steep gradient due to peculiar isovelocities to the south and where the receding side is much more normal, with an almost constant velocity of ∼100 km s^{-1}. We show the RC of HCG 96a from NSOMT2000 and from Keel (1996). Data from Keel (1996) have been taken using a PA = 148°, close to our choice of PA = 132°, but NSOMT2000 used a very different PA of 90°. When we mimic a slit of PA = 90° using our data, we do reproduce the curve derived by NSOMT2000. The curve determined by Keel (1996) is in better agreement with ours, even if the velocity amplitude is lower than ours in the receding part. In the approaching side the agreement is excellent, confirming the steep decreasing curve beyond −20 arcsec (11.4 kpc). Verdes-Montenegro et al. (1997) also published a velocity curve for HCG 96a, but using a PA = 66°, corresponding to the direction that joins the centers of the two galaxies HCG 96a and HCG 96c. Using our data and simulating a long slit along the same axis, we found a curve similar to that presented by Verdes-Montenegro et al. (1997), but the velocity amplitudes we find are lower by ∼50 km s^{-1} than those found in that paper.

The monochromatic map of HCG 96c does not show very strong emission regions. The continuum map shows very peaked emission in the center. The velocity field has a peculiar shape, where the isovelocities are not regular. The velocity difference between the isovelocities in the southwestern part of HCG 96c and the eastern part of HCG 96a is less than 20 km s^{-1}, suggesting a possible physical connection between the two objects. However, the central velocity we found for HCG 96c is ∼150 km s^{-1} lower than the published systemic velocity (Verdes-Montenegro et al. 1997; Hickson 1993). The RC of HCG 96c is very disturbed, with a sinusoidal shape. No possible match between receding and approaching sides of the RC could be found for this galaxy.

The monochromatic map of HCG 96d shows regular emission with no clumpy structure, as we could expect for an Im galaxy. Images made by Verdes-Montenegro et al. (1997) and Hickson (1993) show two other nuclei for this galaxy. However, we could not find any equivalent components in Hα. The continuum map shows significantly weaker continuum than for the two other members. The velocity field shows regular isovelocities except to the northern side, located close to the knot quoted as "A" by Verdes-Montenegro et al. (1997). The RC we present shows a nice match between the two sides till 5 arcsec (2.8 kpc), after which the receding side velocities present a large gradient (at the position of knot A) and the velocities in the approaching side remain almost constant.

4. General discussion and conclusions

4.1. A census of the interaction-related properties of the galaxies

One of the main reasons why it is important to have the full kinematic information for each compact-group member is to have some insight about the possible interaction history of the galaxy. Mendes de Oliveira et al. (1998) described several interaction indicators and listed those present in the galaxies studied by them. Similarly, in Table 5, we list different indicators for all the galaxies studied here. Different interaction scenarios, depending on the strength of the encounter and the morphological types of the interacting systems, will leave different signatures on the velocity fields of the galaxies. Indicators like *highly disturbed velocity field, double nuclei and double kinematic gas component* are used to show evidences for strong interactions or merger. Other indicators such as *warping, stellar and gas major axis misalignment, tidal tail, high IR luminosity and central activity* are used to show indications of collisions which do not lead to merging. We have added here a new indicator: the high discrepancy between both sides of the rotation curve. It

could appear somewhat redundant with the velocity field as a purely circular rotation curve is the zero momentum of the velocity field; nevertheless, exactly for that reason, it is easier to analyze. In some cases, the rotation curve can be rather symmetric and the velocity field highly disturbed, the reverse being much less common. Indeed, if the potential well is axisymmetric, the velocity field is regular and symmetric and both sides of the rotation curves match. What do we mean by highly disturbed velocity field and rotation curve? Non axisymmetric potential wells are observed in isolated as well is interacting galaxies. In isolated galaxies, it is due to "intrinsic" reasons: e.g. the presence of a non axisymmetric structure like a bar, a triaxial bulge and/or a halo, a warp of the disk. In interacting galaxies, non axisymmetric potential wells could naturally also be a consequence of "intrinsic" features but could also be due to external interactions with other galaxies like tidal forces and merging. Moreover, these "intrinsic" features, when they are already present in a galaxy, they are usually amplified by the interaction and can be induced if they were not present. Nevertheless, in the "intrinsic" case, the distortions of the velocity field are relatively weak and, even if both sides of the rotation curve do not match, the disagreement is generally relatively weak. In contrast, in the case of strong interactions and merging, the velocity field could be highly disturbed and the disagreement between both sides of the rotation curve could be large. A two-body tidal interaction like the one produced by the system Earth-Moon is supposed to add an axisymmetric component to the resulting force and the distortions in the rotation curve should be axisymmetric as well. In galactic tidal interactions, the problem is different because the time of propagation of the interaction as well as the duration of the event have to be taken into account. These parameters lead to non axisymmetric morphology and kinematics as described thirty years ago by the first simulations by Toomre & Toomre (1972). As a consequence, strong tidal interaction and a fortiori merging (interpenetration of the stellar disks which induces torques) lead to highly disturbed velocity field and rotation curves. In that case our corresponding "indicator" will be "on". Therefore, the degrees of disturbance of the velocity field and of the rotation curves are excellent indicators of the degree of interaction and merging. Nevertheless, one should keep in mind that an unique classification and identification pointing unambiguously to the cause of some kind of interaction from outside or from inside the galaxy is a difficult problem who is addressed here with caution.

4.2. Groups: HCG 10 – HCG 19 – HCG 87 – HCG 91 – HCG 96

In Table 5 we list the nine indicators for interactions and merging and we mark which galaxies show evidence of such an indicator.

We observed three of the four members of HCG 10 (HCG 10a, HCG 10c and HCG 10d). HCG 10a should be taken with caution due to the weakness of the Hα emission for this galaxy. HCG 10c shows six indicators for interactions. Only one is in favour of a merger process. Also the misalignment between gas and stellar major axis indicates that this member had an interaction in the past. On the other hand, HCG 10d does not show any indicators for a past or present interaction. HCG 10 a and c show extended spiral arms that could be in fact tidal tails. HCG 10c is the most disturbed of the observed galaxies, suggesting it is the most evolved of the group in contrast with HCG 10d, which seems to be untouched and which could be a new object entering the group.

We observed the three accordant members of HCG 19 (HCC 19a, HCC 19b and HCC 19c). HCG 19a and HCG 19b show respectively four and five indicators in favour for past/ongoing interactions and HCG 19c only three. The common property of HCG 19a and HCG 19b is the very weak emission they show. Also both show disturbed velocity fields and HCG 19c, even if its velocity field is regular, has a disturbed extension to the west. None of the group members show evidence that it may be the result of a merger. HCG 19c may play the role of a gas tank fuelling HCG 19a. Despite the relative low number of positive interaction indicators, HCG 19 seems to be an evolved group: HCG 19b may have gone through a starburst phase consuming the HI around it and HCG 19c could be in the process of fuelling HCG 19a with gas.

We observed two of the four members of HCG 87 (HCC 87a and HCC 87c), HCG 87b does not show gas in emission and HCG 87d is a background object. This group shows evidences for an interaction scenario but not for a merging one. Nevertheless, HCG 87c has five positive indicators for interaction and the central activity for the three group members could be the result of gas exchange between the galaxies. HCG 87a is difficult to analyze because of the absorption due to the dust and the projection effects.

We observed three of the four members of HCG 91 (HCC 91a, HCG 91c and HCC 91d). HCG 91a exhibits a large tail in direction of HCG 91c and this galaxy presents six positive indicators for past/ongoing interactions. The velocity field is strongly disturbed due to a huge tail having an almost constant velocity. On the other hand HCG 91c shows a double gaseous component strongly suggesting a past interaction with four positive indicators. We could not find emission in HCG 91d neither a connection of this galaxy with HCG 91a. A probable scenario for this group is the passage of HCG 91c through the group forming the tail of HCG 91a. The HI distribution published by Barnes & Webster (2001) seems to support this idea, because it shows a bridge between the two galaxies.

We observed three of the four members of HCG 96 (HCC 96a, HCG 96c and HCC 96d). HCG 96a shows seven positive indicators for past or present interaction. There is a connection between HCG 96a and HCG 96c. HCG 96c and HCG 96d show four positive indicators. These three galaxies present highly disturbed velocity fields and HCG 96d shows a central double nuclei. This argues in favor of this group being highly evolved.

In a following paper, the data presented here will be interpreted, along with those shown in other previous publications which analyzed other compact group galaxies (Amram et al. 1998; Mendes de Oliveira et al. 1998, 2001; Plana et al. 1998, 1999, 2000, 2003) in order to determine an evolutionary sequence of groups in different dynamical stages, in an attempt

Table 5. Interaction Indicators. Description of the columns: (1) Highly disturbed velocity field. (2) Disagreement between both sides of the rotation curve. (3) Central double nuclei. (4) Double kinematic gas component. (5) Changing position angle (PA) along major axis (MA). Rotation of external isophotes. (6) Gaseous vs stellar MA misalignment. The indicator is "on" if the ranges of values do not intersect. (7) Tidal Tail, shell, filaments. (8) High L_{IR}. (9) Central activity. The symbol "+" means that the indicator is "on" otherwise the symbol is "–". The symbol "×" means that the data do not allow measurements.

Interaction Indicator / Group Member	1	2	3	4	5	6	7	8	9
HCG 10a	×	×	–	×	×	×	×	?	+
HCG 10c	+	+	–	–	+	+	+	+	–
HCG 10d	–	+	–	–	–	–	–	–	–
HCG 19a	+	+	–	–	+	+	–	–	–
HCG 19b	+	+	–	–	+	–	–	+	+
HCG 19c	–	+	–	–	–	+	+	–	–
HCG 87a	×	×	×	–	–	–	+	–	+
HCG 87c	+	+	–	–	+	+	–	–	+
- HCG 91a	+	+	–	–	+	+	+	+	–
HCG 91c	+	–	–	+	+	+	–	–	–
HCG 96a	+	+	–	–	+	+	+	+	+
HCG 96c	+	+	–	–	–	–	–	+	+
HCG 96d	+	+	+	–	–	+	–	–	–

to date compact groups, from the least evolved ones to those close to total merging.

Acknowledgements. The authors thank J. L. Gach for helping during the observations. The authors also thank the referee for his/her comments. H.P. acknolwedges the financial support of the Brazilian CNPQ, under contract 150089/98-8. H.P. thanks Brazillian PRONEX program, for financial help to attend the conference "Galaxies: the Third Dimension" in Cozumel (Mexico), Dec. 3–7 2001. CMdO acknowledges funding from FAPESP, Cnpq and PRONEX. This research has made use of the NASA/IPAC Extragalactic Data Base (NED) which is operated by the Jet Propulsion Laboratory, California Institute of Technology, under contract with the National Aeronautics and Space Administration.

References

Allam, S., Assendorp, R., Longo, G., Braun, M., & Richter, G. 1996, A&AS, 117, 39
Amram, P., Balkowski, C., Boulesteix, J., et al. 1996, A&A, 310, 737
Amram, P., & Garrido, O. 2002, in Galaxies: the Third Dimension, Cozumel, Mexico 3–7 December 2001, Conf. Ser. of the Astronomical Society of the Pacific, ed. M. Rosado, L. Binette, & L. Arias
Amram, P., Mendes de Oliveira, C., Boulesteix, J., & Balkowski, C. 1998, A&A, 330, 881
Barnes, D. G., & Webster, R. L. 2001, MNRAS, 324, 859
Barnes, J. 1989, Nature, 338, 123
Barnes, J., & Hernquist, L. 1992, Nature, 360, 715
Barnes, J., & Hernquist, L. 1996, ApJ, 471, 115
Boselli, A., Mendes de Oliveira, C., Balkowski, C., Cayatte, V., & Casoli, F. 1996, A&A, 314, 738
Boulesteix, J. 2002, User Manual of ADHOCw reduction Package, Publication of Observatoire de Marseille, updated version `http://www-obs.cnrs-mrs.fr/adhoc`
Bureau, M., & Freeman, K. C. 1999, AJ, 118, 126
Coziol, R., Ribeiro, A. L. B., de Carvalho, R., & Capelato, H. V. 1998, ApJ, 493, 563
de Carvalho, R. R., Ribeiro, A. L. B., Capelato, H. V., & Zepf, S. E. 1997, ApJS, 110, 1
Ebeling, H., Voges, W., & Boehringer, H. 1994, ApJ, 436, 44
English, J., Hunsberger, S., Charlton, J., et al. 1999, Am. Astron. Soc. Meet., 195, #136.04
Garrido, O., Marcelin, M., Amram, P., & Boulesteix, J. 2002, A&A, 387, 821
Garrido, O., Marcelin, M., Amram, P., & Boissin, O. 2003, A&A, 399, 51
Hickson, P. 1982, ApJ, 255, 382
Hickson, P. 1993, ApL&C, 29, 1
Hickson, P., Kindl, E., & Auman, J. 1989, ApJS, 70, 687
Hickson, P., Mendes de Oliveira, C., Huchra, J. P., & Palumbo, G. G. C. 1992, ApJ, 399, 353
Jarvis, J. 1986, AJ, 91, 65
Keel, W. C. 1996, ApJS, 106, 27
Laval, A., Boulesteix, J., Georgelin, Y. P., Georgelin, Y. M., & Marcelin, M. 1987, A&A, 175, 199
Leon, S., Combes, F., & Menon, T. K. 1998, A&A, 330, 37
Mendes de Oliveira, C., Plana, H., Amram, P., Balkowski, C., & Boulesteix, J. 1998, ApJ, 507, 691
Mendes de Oliveira, C., Plana, H., Amram, P., Balkowski, C., & Bolte, M. 2001, AJ, 121, 2524
Mihos, J. C., Walker, I. R., Hernquist, L., Mendes de Oliveira, C., & Bolte, M. 1995, ApJ, 447, L87
Mirabel, I. F., & Wilson, A. S. 1984, ApJ, 277, 92
Nishiura, S., Shimada, M., Ohyama, Y., Murayama, T., & Taniguchi, Y. 2000, AJ, 120, 169 (NSOMT2000)
Paturel, G., Andernach, H., Bottinelli, L., et al. 1997, A&AS, 124, 109
Pildis, R. A., Bregman, J. N., & Schombert, J. M. 1995, AJ, 110, 1498
Plana, H., Mendes de Oliveira, C., Amram, P., & Boulesteix, J. 1998, AJ, 116, 2123
Plana, H., Mendes de Oliveira, C., Amram, P., et al. 1999, ApJ, 516, L69
Plana, H., Amram, P., Mendes de Oliveira, C., & Balkowski, C. 2000, AJ, 120, 621
Plana, H., Amram, P., Mendes de Oliveira, C., Balkowski, C., & Boulesteix, J. 2003, AJ, submitted
Ponman, T. J., Bourner, P. D. J., Ebeling, H., & Bohringer, H. 1996, MNRAS, 283, 690
Ribeiro, A. L. B., de Carvalho, R. R., Capelato, H. V., & Zepf, S. E. 1998, ApJ, 487, 72
Rubin, V. C., Hunter, D. A., & Ford, W. K. Jr. 1991, ApJS, 76, 153 (RHF1991)
Shaw, M., Dettmar, R., & Barteldrees, A. 1990, A&A, 240, 36
Shimada, M., Ohyama, Y., Nishiura, S., Murayama, T., & Taniguchi, Y. 2000, AJ, 119, 2664
Toomre, A., & Toomre, J. 1972, ApJ, 178, 623
Verdes-Montenegro, L., Yun, M. S., Perea, J., del Olmo, A., & Ho, P. T. P. 1998, ApJ, 497, 89
Verdes-Montenegro, L., del Olmo, A., Perea, J., et al. 1997, A&A, 321, 409
Verdes-Montenegro, L., Yun, M. S., Williams, B. A., et al. 2001, A&A, 377, 812
Williams, B. A. 1985, ApJ, 290, 462